

Relative Attribute Classification with Deep Rank SVM

Sara Atito Ali Ahmed and Berrin Yanikoglu
Faculty of Engineering and Natural Sciences
Sabanci University
Istanbul, Turkey 34956
{saraatito,berrin}@sabanciuniv.edu

Abstract—Relative attributes indicate the strength of a particular attribute between image pairs. We introduce a deep Siamese network with rank SVM loss function, called Deep Rank SVM (DRSVM), in order to decide which one of a pair of images has a stronger presence of a specific attribute. The network is trained in an end-to-end fashion to jointly learn the visual features and the ranking function. We demonstrate the effectiveness of our approach against the state-of-the-art methods on four image benchmark datasets: LFW-10, PubFig, UTZap50K-lexi and UTZap50K-2 datasets. DRSVM surpasses state-of-the-art in terms of the average accuracy across attributes, on three of the four image benchmark datasets.

I. INTRODUCTION

Identification and retrieval of images and videos with certain visual attributes are of interest in many real-world applications, such as image search/retrieval [1], [2], video retrieval [3], image/video captioning [4], [5], face verification [6], and zero-shot learning [7], [8]. Visual attribute learning is studied in particular for binary attributes that indicate the presence or absence of a certain semantic attribute (smiley, wearing eye glasses, etc.) [9], [10].

Parikh and Grauman [11] introduced *relative attributes* with a formulation similar to that of Support Vector Machines (SVMs). The goal of relative attribute learning is to learn a function which predicts the relative strengths of a pair of images regarding a given attribute (e.g. which picture is more smiling?). The network should be able to answer the comparisons, with more/less/equal of the presence of a specific attribute. Figure 1 shows the comparison for two separate data sets, for the attributes *mouth-open* and *sparty* from the LFW10 and UTZap50K-2 datasets.

After the introduction of the problem, subsequent research approached the problem using either traditional features or deep learning approaches, as discussed in Section II.

In this paper, we present a deep learning system that can compare the given two images in terms of their strength regarding a particular attribute. Specifically, we propose a convolutional Siamese network using rank SVM loss function for the relative attribute problem. The main contributions of our proposed model are summarized as follows:

- Proposing an end-to-end deep learning framework in which the network jointly learns the visual features and the rank SVM function, for relative attribute classification.

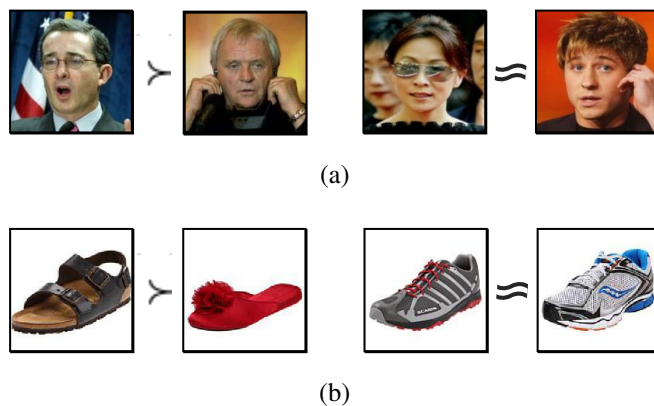


Fig. 1: Samples of visual relative attributes from the training dataset. (a) Shows random samples from LFW10 dataset of *mouth-open* attribute, and (b) Shows random samples from UTZap50K-2 dataset of *sparty* attribute.

- Demonstrating the effectiveness of the proposed framework by comparing to our baseline [12], with improvements of 6%, 3%, 2.65%, and 1% in average ranking accuracy for LFW-10, PubFig, UTZap50K-lexi, and UTZap50K-2 datasets, respectively.
- Surpassing the state-of-the-art results in LFW-10, PubFig, and UTZap50K-lexi datasets by about 2%, 0.2%, and 0.87% and obtaining slightly lower results in UTZap50K-2 dataset.

The rest of this paper is organized as follows. A review of literature is presented in Section II. Section III introduces our proposed method together using the deep rank SVM objective function. Description of the employed datasets, implementation details, along with extensive experimental results are discussed in Section IV. Finally, the paper concludes in Section V.

II. RELATED WORKS

The relative attribute learning problem has attracted significant attention, with researchers approaching it first using traditional approaches and later using deep learning approaches. Traditional and hand-crafted features are first used in [11], [13], [14], [15], [16]; however, more recently, deep convolutional neural networks are used to jointly learn the features



Fig. 2: Overall Deep Rank SVM architecture. The network for a given attribute takes a pair of images $(\mathbf{x}_i, \mathbf{x}_j)$ as input and outputs 1 if \mathbf{x}_i shows the given attribute more strongly, compared to \mathbf{x}_j ; 0 otherwise.

and the ranking function in an end-to-end fashion [12], [17], [18], [19].

A. Traditional Approaches

Parikh and Grauman [11] first proposed relative attributes where they used the GIST descriptor [20] and color histogram features, together with a constrained optimization formulation similar to that of SVMs.

Later, Li et al. [13], introduced non-linearity by using the relative forest algorithm to capture more accurate semantic relationships. More recently, Yu and Grauman [16], developed a Bayesian local learning strategy to infer when images are indistinguishable for a given attribute in a probabilistic, local learning manner.

B. Deep Learning Approaches

Hand-crafted feature representation may not be the best to capture the relevant visual features to describe relative attributes. As with many other visual recognition problems, deep learning approaches significantly outperform approaches that are based on hand-crafted features followed by shallow models.

Souri et al. [12] introduced RankNet, which is a convolutional neural network based on the architecture of VGG-16 [21]. A ranking layer is included to rank the strength of an attribute in the given pair of images based on the extracted features in an end-to-end fashion.

Using a similar approach, Yang et al. [18] proposed a DRA model which consists of five convolutional neural layers and five fully connected layers followed by a relative loss function.

Singh and Lee [17] trained a Siamese network based on AlexNet [22], with a pairwise ranking loss. The network consists of two branches, each branch consists of a localization module and a ranking module.

In Zhuang et al. [19], cross-image representation is considered via deep attentive cross-image representation learning (DACRL) model: an end-to-end convolutional neural network

which takes a pair of images as input, and outputs a posterior probability that indicates the relative strengths of a specific attribute, based on cross-image representation learning.

Our work most resembles [12], except for the loss function. As one of our contributions is embedding the SVM loss into the network, we compare our results to this system as the baseline; as well as newer work that achieved state-of-art results [17] [19].

III. DEEP RANK SVM

We introduce Deep Rank SVM (DRSVM), a convolutional Siamese network trained with the rank SVM objective function. While rank SVM formulation was proposed before [23], this is the first time it is incorporated into a deep network architecture as a loss, to the best of our knowledge.

Following Parikh and Grauman’s [11] notation, training images consist of a set of ordered image-pairs $\mathbf{O}_m = (\mathbf{x}_i, \mathbf{x}_j)$ and a set of un-ordered image-pairs $\mathbf{S}_m = (\mathbf{x}_i, \mathbf{x}_j)$ for every attribute m of a set of M attributes. $(\mathbf{x}_i, \mathbf{x}_j) \in \mathbf{O}_m$ when the presence of attribute m in \mathbf{x}_i is stronger than the presence of attribute m in \mathbf{x}_j and $(\mathbf{x}_i, \mathbf{x}_j) \in \mathbf{S}_m$ when \mathbf{x}_i and \mathbf{x}_j have similar presence strength of attribute m .

With these notations, we can formulate the problem as learning the deep attribute representation $\mathbf{h}(\mathbf{x})$ of an image, for a specific attribute m that satisfies the following constraints:

$$\begin{aligned} \mathbf{w}_m^T \mathbf{h}(\mathbf{x}_i) &> \mathbf{w}_m^T \mathbf{h}(\mathbf{x}_j); & \forall (\mathbf{x}_i, \mathbf{x}_j) \in \mathbf{O}_m \\ \mathbf{w}_m^T \mathbf{h}(\mathbf{x}_i) &= \mathbf{w}_m^T \mathbf{h}(\mathbf{x}_j); & \forall (\mathbf{x}_i, \mathbf{x}_j) \in \mathbf{S}_m \end{aligned} \quad (1)$$

In this work, we use the VGG-16 architecture [21] as the base of a Siamese network to jointly learn the deep attribute representation $\mathbf{h}(\mathbf{x})$ and the weights \mathbf{w}_m to rank the two input images for the given attribute m . The network is illustrated in Figure 2. As seen in this figure, the output of the two branches of the network are 1,000 dimensional each. An additional layer is added to carry out the difference between the feature representations, $\mathbf{h}(\mathbf{x}_i)$ and $\mathbf{h}(\mathbf{x}_j)$; followed by an

output node that computes the weighted differences between the two representations.

For the objective function, we use the rank SVM formulation proposed in [11]; however unlike their use of the GIST features, we aimed to jointly learn the visual features and the rank SVM function, in a deep convolutional network. Details of the whole architecture are described in Section IV-B.

The input to the rank SVM function is the deep attribute representations $\mathbf{h}(\mathbf{x}_i)$ and $\mathbf{h}(\mathbf{x}_j)$, computed by the Siamese network for the image-pair, \mathbf{x}_i and \mathbf{x}_j . The rank SVM optimization function for relative attributes is defined as in [11]:

$$\begin{aligned} \min \quad & \frac{1}{2} \mathbf{w}_m^T \mathbf{w}_m + C_1 \sum \xi_{ij}^2 + C_2 \sum \gamma_{ij}^2 \\ \text{subject to} \quad & \mathbf{w}_m^T (\mathbf{h}(\mathbf{x}_i) - \mathbf{h}(\mathbf{x}_j)) \geq 1 - \xi_{ij} \quad \forall (i, j) \in \mathbf{O}_m \\ & |\mathbf{w}_m^T (\mathbf{h}(\mathbf{x}_i) - \mathbf{h}(\mathbf{x}_j))| \leq \gamma_{ij} \quad \forall (i, j) \in \mathbf{S}_m \\ & \xi_{ij} \geq 0, \gamma_{ij} \geq 0 \end{aligned} \quad (2)$$

where \mathbf{w}_m is the trainable weights of the ranking layer, the first term maximizes the margin, while the second and third terms are there to enforce the soft margin of ordered/unordered image-pairs on the training images. We also used quadratic terms for the soft error as in [11]. C_1 and C_2 are the trade-off constants between maximizing the margin and satisfying the pairwise relative constraints. We choose C_1 and C_2 to be equal as done in [11] and with the value of 0.1.

We then obtain the corresponding unconstrained optimization problem by combining the constraints on the slack variables ξ_{ij} and γ_{ij} , as:

$$\begin{aligned} \min_{\mathbf{w}_m} \quad & \frac{1}{2} \mathbf{w}_m^T \mathbf{w}_m + C_1 \sum_{(i,j) \in \mathbf{O}_m} \max(0, 1 - \mathbf{w}_m^T (\mathbf{h}(\mathbf{x}_i) - \mathbf{h}(\mathbf{x}_j)))^2 \\ & + C_2 \sum_{(i,j) \in \mathbf{S}_m} (\mathbf{w}_m^T (\mathbf{h}(\mathbf{x}_i) - \mathbf{h}(\mathbf{x}_j)))^2 \end{aligned} \quad (3)$$

As suggested in [24], the objective function is calculated with no bias term to avoid learning the constant function mapping directly to the relative ordering.

IV. EXPERIMENTAL EVALUATION

We evaluate the effectiveness of our approach on the publicly available datasets for relative attributes, described in Section IV-A. Our results are compared to the results of several systems that report accuracy as performance measurement, namely Rank SVM [11], FG-LP [14], spatial Extent [15], DeepSTN [17], DRA [18], and DACRL [19].

We consider the RankNet system proposed in [12] as our baseline. We used the same network (VGG-16 pre-trained on ILSVRC 2014) and the same data augmentation techniques, but the proposed rank SVM loss function was used instead of the cross-entropy loss used in RankNet. In this way we aimed to evaluate the effectiveness of using the SVM formulation with our deep learning framework.

In Section IV-B, the network and implementation details are explained. In Section IV-C, the performance of our proposed method is shown along with a comparison with the baseline and other state-of-the-art systems.

A. Datasets

Our proposed approach is evaluated on four different datasets from distinctive areas for comprehensive evaluation.

- 1) **LFW-10 Dataset [25]**: The dataset is a subset of the Labels Faces in the Wild (LFW) dataset [26]. It consists of 2,000 images with 10 different face attributes (refer to Table I). For each attribute, a random subset of 500 pairs of images have been annotated for training and testing sets.
- 2) **Public Figure Face Dataset [11]**: PubFig dataset consists of 772 images from 8 different identities with 11 semantic attributes (refer to Table II). The ordering of the samples are annotated at the category level; in other words, all images with the same identity are ranked higher, equal, or lower than all images belonging to another identity with respect to a specific attribute. For instance, a person is said to have longer hair than another person, even if this may not be true in all of their photographs. This short-cut in annotation will result in label inconsistencies.
- 3) **UTZap50K-2 Dataset [14]**: Large shoe dataset consists of 50,025 images collected from Zappos.com. It consists of 4 shoe attributes: open, pointy, sporty, and comfort (refer to Table IV). After pruning out pairs with low confidence or agreement, the human-annotated examples consist of approximately 1,500-1,800 training image-pairs for each attribute and in total 4,334 image-pairs for testing.
- 4) **Zappos50K-lexi Dataset [27]**: It is based on UTZap50K dataset [14] with 10 additional fine-grained relative attributes: comfort, casual, simple, sporty, colorful, durable, supportive, bold, sleek, and open (refer to Table III). The dataset consists of approximately 1,300-2,100 image-pairs for each attribute.

In all of our experiments, we have used the provided training/testing split by the original publishers of the datasets.

B. Implementation Details

We chose the VGG-16 model to be our base architecture to have a fair comparison with our baseline [12], which uses the same architecture.

The input to the model is two 224×224 RGB images similar to [12]. The output of the two branches of Siamese network $\mathbf{h}(\mathbf{x}_i)$ and $\mathbf{h}(\mathbf{x}_j)$ are 1,000 dimensional each, as illustrated in Figure 2. The weight initialization for the output node is sampled from a zero-mean Gaussian distribution with a standard deviation of 0.01.

To implement and fine-tune our architecture, we have used the pre-trained VGG-16 provided by Keras framework. The last added weights \mathbf{w}_m of the ranking layer is initialized using the Xavier method without bias term. For training, stochastic gradient descent with RMSProp optimizer is used with a mini-batch size of 48 image-pairs. A unified learning rate is set to 10^{-5} for all of the layers. The training images are shuffled after every epoch.

| Method | Bald Head | Dark Hair | Eyes Open | Good Looking | Mascu. Looking | Mouth Open | Smile | Teeth | Fore-head | Young | Mean |
|--------------------------------|--------------|--------------|--------------|--------------|----------------|--------------|--------------|--------------|--------------|--------------|---------------|
| FG-LP [14] | 67.90 | 73.60 | 49.60 | 64.70 | 70.10 | 53.40 | 59.70 | 53.50 | 65.60 | 66.20 | 62.43% |
| Spatial Extent [15] | 83.21 | 88.13 | 82.71 | 72.76 | 93.68 | 88.26 | 86.16 | 86.46 | 90.23 | 75.05 | 84.67% |
| RankNet [12] | 81.14 | 88.92 | 74.44 | 70.28 | 98.08 | 85.46 | 82.49 | 82.77 | 81.90 | 76.33 | 82.18% |
| DeepSTN [17] | 83.94 | 92.58 | 90.23 | 71.21 | 96.55 | 91.28 | 84.75 | 89.85 | 87.89 | 80.81 | 86.91% |
| DACRL [19] (without Attention) | 83.21 | 91.99 | 87.97 | 69.97 | 97.70 | 89.93 | 85.03 | 88.00 | 89.45 | 74.84 | 85.81% |
| DACRL [19] | 85.04 | 92.58 | 90.23 | 70.28 | 98.28 | 91.28 | 85.03 | 89.23 | 90.63 | 76.55 | 86.91% |
| DRSVM (proposed) | 90.75 | 92.67 | 86.54 | 71.21 | 95.05 | 92.67 | 88.64 | 91.80 | 90.84 | 81.02 | 88.12% |

TABLE I: State-of-the-art accuracies on LFW-10 dataset compared with the results obtained in this work. Bold figures indicate the best results.

| Method | Male | White | Young | Smile | Chubby | Fore-head | Bushy Eyebrow | Narrow Eyes | Pointy Nose | Big Lips | Round Face | Mean |
|--------------------------------|--------------|--------------|--------------|--------------|--------------|--------------|---------------|--------------|--------------|--------------|--------------|---------------|
| FG-LP [14] | 91.77 | 87.43 | 91.87 | 87.00 | 87.37 | 94.00 | 89.83 | 91.40 | 89.07 | 90.43 | 86.70 | 89.72% |
| RankNet [12] | 95.50 | 94.60 | 94.33 | 95.36 | 92.32 | 97.28 | 94.53 | 93.19 | 94.24 | 93.62 | 94.76 | 94.42% |
| DRA [18] | 90.82 | 87.12 | 91.49 | 92.68 | 89.30 | 94.39 | 90.19 | 90.60 | 91.03 | 90.35 | 91.99 | 90.91% |
| DACRL [19] (without Attention) | 97.70 | 97.82 | 97.10 | 97.03 | 97.05 | 98.30 | 97.36 | 97.99 | 97.26 | 94.36 | 98.04 | 97.27% |
| DACRL [19] | 96.49 | 97.80 | 97.96 | 97.42 | 97.22 | 98.05 | 97.48 | 96.91 | 97.74 | 96.83 | 96.27 | 97.29% |
| DRSVM (proposed) | 97.74 | 98.61 | 96.32 | 96.14 | 94.47 | 98.75 | 98.68 | 97.28 | 99.31 | 98.24 | 96.89 | 97.49% |

TABLE II: Comparison of the state-of-the-art accuracies on the PubFig dataset.

| Method | Comfort | Casual | Simple | Sporty | Colorful | Durable | Supportive | Bold | Sleek | Open | Mean |
|--------------------------------|--------------|--------------|--------------|--------------|--------------|--------------|--------------|--------------|--------------|--------------|---------------|
| RankNet [12] | 90.48 | 90.43 | 90.40 | 93.31 | 95.43 | 90.47 | 91.98 | 91.53 | 86.31 | 82.53 | 90.29% |
| DACRL [19] (without Attention) | 91.88 | 94.44 | 89.93 | 93.01 | 97.33 | 92.65 | 92.65 | 91.12 | 89.24 | 87.90 | 92.02% |
| DACRL [19] | 91.88 | 91.36 | 90.16 | 94.22 | 95.81 | 92.33 | 92.65 | 92.56 | 90.71 | 88.98 | 92.07% |
| DRSVM (proposed) | 91.59 | 95.37 | 90.91 | 96.57 | 95.95 | 93.31 | 94.98 | 91.47 | 89.30 | 89.99 | 92.94% |

TABLE III: Comparison of the state-of-the-art accuracies on the UTZap50K-lexi dataset.

| Method | Open | Pointy | Sporty | Comfort | Mean |
|--------------------------------|--------------|--------------|--------------|--------------|---------------|
| RankSVM [11] | 60.18 | 59.56 | 62.70 | 64.04 | 61.62% |
| FG-LP [14] | 74.91 | 63.74 | 64.54 | 62.51 | 66.43% |
| RankNet [12] | 73.45 | 68.20 | 73.07 | 70.31 | 71.26% |
| DACRL [19] (without Attention) | 75.45 | 69.80 | 73.78 | 68.54 | 71.89% |
| DACRL [19] | 75.66 | 70.65 | 73.87 | 69.56 | 72.44% |
| DRSVM (proposed) | 74.09 | 70.90 | 72.95 | 71.20 | 72.29% |

TABLE IV: Comparison of the state-of-the-art accuracies on the UTZap50K-2 dataset.

A separate network for each attribute is trained. For LFW-10, UTZap50K-2, and UTZap50K-lexi datasets, we trained our model for 500, 200, and 200 epochs for each attribute, respectively. For PubFig dataset, the relative attributes are annotated at the category-level manner; hence one epoch contains large number of image-pairs, that is the combination of all of the images in the dataset. Therefore, we trained the model for 10,000 iterations where in every iteration a random selection of 48 image-pairs are chosen from the dataset, and ground-truth labels are assigned based on their categories.

Advanced data augmentation techniques have proven to improve performance in many studies specially for deep learning. However, to resemble our baseline and show the effectiveness of incorporating Rank SVM loss function to the deep learning, only simple on-the-fly data augmentation techniques are applied during training, namely rotation [-15, 15], horizontal flipping, and random cropping.

C. Results

We compare the performance of the proposed Deep Rank SVM model (DRSVM) with our baseline [12] and state-of-the-art, on four different datasets, in Tables I-IV. The reported performance figures are accuracies over correctly ordered pairs (excluding similar pairs), in line with the literature.

Table I shows the results on the LFW-10 dataset where we outperform our baseline [12] by about 6% on average. We can attribute this to the use of the rank SVM loss as the loss function, as this is the main difference between our model and the baseline. Our results surpass the average accuracy by 1.2% points over the state-of-the-art [19], with best performance on 7 of the 10 attributes.

Table II shows the results on the PubFig dataset where our system improves over the baseline [12] by 3% points and obtains the best results on 8 out of 11 attributes compared to state-of-art [19]. The gain on this dataset is marginal (0.2%) which may be due to the category base annotation that may

result in annotation inconsistencies, as discussed in Section IV-A.

Table III shows the results on the UTZap50K-lexi dataset where we outperform the baseline by 2.65%. Furthermore, we improve the average accuracy by 0.87% over the state-of-the-art [19] and obtain the best results in 6 out of the 10 attributes.

Finally, Table IV shows the results on the UTZap50K-2 dataset where we outperform the baseline by 1%, but slightly underperform the state-of-art [19] by 0.15% (72.29% vs 72.44%), while obtaining best results in 2 out of 4 attributes.

D. Discussion

The reported results in Tables I-III show that we outperformed our baseline [12] on the four employed datasets, LFW-10, PubFig, UTZap50K-lexi, and UTZap50K-2 by 6%, 3%, 2.65%, and 1% points respectively. This shows the effectiveness of using the rank SVM loss with the deep learning approach, for the relative attribute learning problem.

Furthermore, we surpassed the state-of-art on the LFW-10, PubFig, and UTZap50K-lexi datasets by 1.2%, 0.2%, and 0.87% points and obtained slightly lower results on the UTZap50K-2 dataset (72.44% versus 72.29%).

To show the effectiveness of incorporating the rank SVM objective function into our deep learning framework, we employed the same architecture used in our baseline [12] and in DACRL [19], namely VGG-16. We expect that the performance of our model will be even higher with a more advanced network (e.g. Inception-ResNet [28] or NasNetLarge [29]) and using heavy data augmentation.

Figure 3 shows some images along with their output prediction values of the respective attribute. Although, our network is trained given only image-pairs, we can see that the network has learned a global ranking of a given attribute.

The trained network is able to localize on the informative regions of the image related to a given attribute, without explicitly being taught to do so during training. We calculate the derivative of the output with respect to a given input and visualize the results of the last convolutional layer as shown in Figure 4. The heat maps visualize the pixels in the images with the most contribution to the ranking prediction of the network.

V. CONCLUSIONS AND FUTURE WORK

In this paper, we proposed the deep rank SVM (DRSVM) network for relative attribute learning, to jointly learn the features and the ranking function in an end-to-end fashion. Our model is evaluated on four benchmarks, LFW-10, PubFig, UTZap50K-lexi and UTZap50K-2 and achieved state-of-the-art performance on LFW-10, PubFig, and UTZap50K-lexi datasets. These results shows the benefit of incorporating and jointly training the network with Rank SVM loss function for relative attributes.

Although the results show the ability of the network to localize on the informative regions in the image, adding a localization module similar to the one used in [19] can contribute to the performance, especially in the existence of

some annotation inconsistencies, as in the case of PubFig dataset.

We believe that the performance can be further improved with a better network (e.g. Inception-ResNet [28] or NasNet-Large [29]) than the one used in this work (VGG-16), as well as using heavy data augmentation. We will add results obtained with a more powerful network in the final version of the manuscript.

Source code of the proposed method is provided in supplementary materials, and will be made public upon acceptance.

ACKNOWLEDGMENT

This work as supported by a grant from The Scientific and Technological Research Council of Turkey (TBTAK) under project number 119E429.

REFERENCES

- [1] A. Kovashka, D. Parikh, and K. Grauman, "Whittlesearch: Interactive image search with relative attribute feedback," *International Journal of Computer Vision*, vol. 115, no. 2, pp. 185–210, 2015.
- [2] A. Kovashka and K. Grauman, "Attributes for image retrieval," in *Visual Attributes*. Springer, 2017, pp. 89–117.
- [3] L. Chen, P. Zhang, and B. Li, "Instructive video retrieval based on hybrid ranking and attribute learning: A case study on surgical skill training," in *Proceedings of the 22nd ACM*, 2014, pp. 1045–1048.
- [4] Y. Pan, T. Yao, H. Li, and T. Mei, "Video captioning with transferred semantic attributes," in *Proceedings of the IEEE conference on computer vision and pattern recognition*, 2017, pp. 6504–6512.
- [5] T. Yao, Y. Pan, Y. Li, Z. Qiu, and T. Mei, "Boosting image captioning with attributes," in *Proceedings of the IEEE International Conference on Computer Vision*, 2017, pp. 4894–4902.
- [6] N. Kumar, A. C. Berg, P. N. Belhumeur, and S. K. Nayar, "Attribute and simile classifiers for face verification," in *2009 IEEE 12th International Conference on Computer Vision*. IEEE, 2009, pp. 365–372.
- [7] Y. Fu, T. Xiang, Y.-G. Jiang, X. Xue, L. Sigal, and S. Gong, "Recent advances in zero-shot recognition: Toward data-efficient understanding of visual content," *IEEE Signal Processing Magazine*, vol. 35, no. 1, pp. 112–125, 2018.
- [8] A. Bansal, K. Sikka, G. Sharma, R. Chellappa, and A. Divakaran, "Zero-shot object detection," in *Proceedings of the European Conference on Computer Vision (ECCV)*, 2018, pp. 384–400.
- [9] S. A. A. Ahmed and B. Yanikoglu, "Within-network ensemble for face attributes classification," in *International Conference on Image Analysis and Processing*. Springer, 2019, pp. 466–476.
- [10] N. Zhuang, Y. Yan, S. Chen, H. Wang, and C. Shen, "Multi-label learning based deep transfer neural network for facial attribute classification," *Pattern Recognition*, vol. 80, pp. 225–240, 2018.
- [11] D. Parikh and K. Grauman, "Relative attributes," in *International Conference on Computer Vision*. IEEE, 2011, pp. 503–510.
- [12] Y. Souri, E. Noury, and E. Adeli, "Deep relative attributes," in *Asian conference on computer vision*. Springer, 2016, pp. 118–133.
- [13] S. Li, S. Shan, and X. Chen, "Relative forest for attribute prediction," in *Asian Conference on Computer Vision*. Springer, 2012, pp. 316–327.
- [14] A. Yu and K. Grauman, "Fine-grained visual comparisons with local learning," in *Proceedings of the IEEE Conference on Computer Vision and Pattern Recognition*, 2014, pp. 192–199.
- [15] F. Xiao and Y. Jae Lee, "Discovering the spatial extent of relative attributes," in *Proceedings of the IEEE International Conference on Computer Vision*, 2015, pp. 1458–1466.
- [16] A. Yu and K. Grauman, "Just noticeable differences in visual attributes," in *Proceedings of the IEEE International Conference on Computer Vision*, 2015, pp. 2416–2424.
- [17] K. K. Singh and Y. J. Lee, "End-to-end localization and ranking for relative attributes," in *European Conference on Computer Vision*. Springer, 2016, pp. 753–769.
- [18] X. Yang, T. Zhang, C. Xu, S. Yan, M. S. Hossain, and A. Ghoneim, "Deep relative attributes," *IEEE Transactions on Multimedia*, vol. 18, no. 9, pp. 1832–1842, 2016.

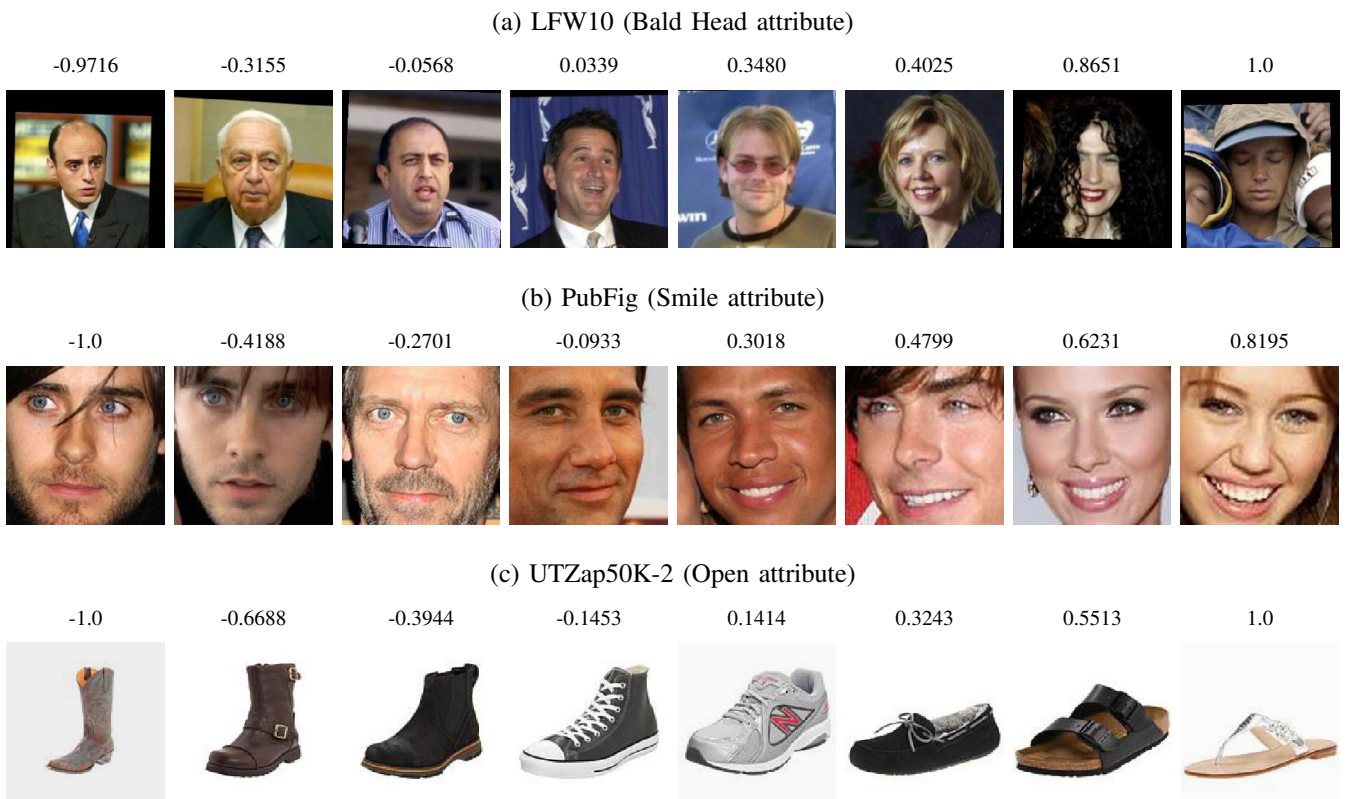


Fig. 3: Sample images ordered according to their output prediction of their associated attribute.

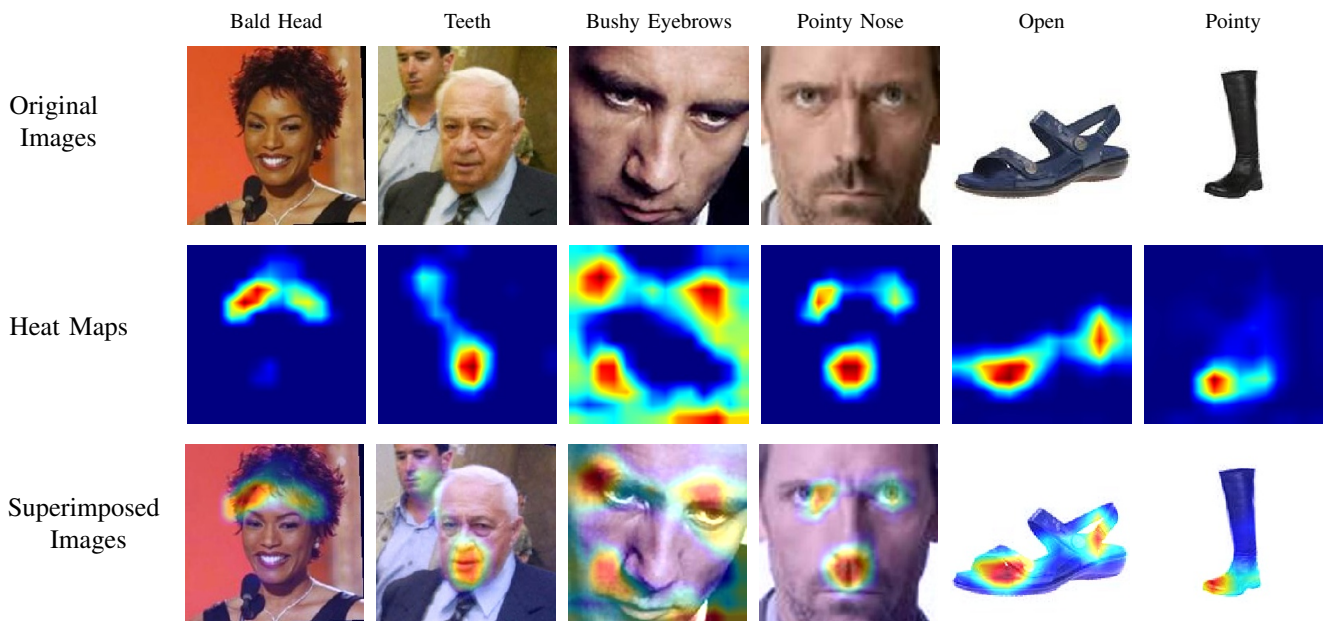


Fig. 4: Class Activation Maps showing the pixels with most contribution to the ranking prediction in (a) Bald Head and Teeth from LFW-10 dataset, (b) Bushy Eyebrows and Pointy Nose from PubFig dataset, and (c) Open and Pointy from UTZap50K-2 dataset.

- [19] Z. Zhang, Y. Li, and Z. Zhang, "Relative attribute learning with deep attentive cross-image representation," in *Asian Conference on Machine Learning*, 2018, pp. 879–892.
- [20] A. Oliva and A. Torralba, "Modeling the shape of the scene: A holistic representation of the spatial envelope," *International journal of computer vision*, vol. 42, no. 3, pp. 145–175, 2001.
- [21] K. Simonyan and A. Zisserman, "Very deep convolutional networks for large-scale image recognition," *arXiv preprint arXiv:1409.1556*, 2014.
- [22] A. Krizhevsky, I. Sutskever, and G. E. Hinton, in *Advances in Neural Information Processing Systems 25*, F. Pereira, C. J. C. Burges, L. Bottou, and K. Q. Weinberger, Eds. Curran Associates, Inc., 2012, pp. 1097–1105.
- [23] T. Joachims, "Optimizing search engines using clickthrough data," in *Proceedings of the Eighth ACM SIGKDD International Conference on Knowledge Discovery and Data Mining*, ser. KDD 02. New York, NY, USA: Association for Computing Machinery, 2002, p. 133142.
- [24] L. Ruff, R. Vandermeulen, N. Goernitz, L. Deecke, S. A. Siddiqui, A. Binder, E. Müller, and M. Kloft, "Deep one-class classification," in *Proceedings of the 35th International Conference on Machine Learning*, ser. Proceedings of Machine Learning Research, J. Dy and A. Krause, Eds., vol. 80. Stockholmsmssan, Stockholm Sweden: PMLR, 10–15 Jul 2018, pp. 4393–4402.
- [25] R. N. Sandeep, Y. Verma, and C. Jawahar, "Relative parts: Distinctive parts for learning relative attributes," in *Proceedings of the IEEE Conference on Computer Vision and Pattern Recognition*, 2014, pp. 3614–3621.
- [26] G. B. Huang, M. Ramesh, T. Berg, and E. Learned-Miller, "Labeled faces in the wild: A database for studying face recognition in unconstrained environments," University of Massachusetts, Amherst, Tech. Rep. 07-49, October 2007.
- [27] A. Yu and K. Grauman, "Semantic jitter: Dense supervision for visual comparisons via synthetic images," in *Proceedings of the IEEE International Conference on Computer Vision*, 2017, pp. 5570–5579.
- [28] C. Szegedy, S. Ioffe, V. Vanhoucke, and A. A. Alemi, "Inception-v4, inception-resnet and the impact of residual connections on learning," in *Thirty-First AAAI Conference on Artificial Intelligence*, 2017.
- [29] B. Zoph, V. Vasudevan, J. Shlens, and Q. V. Le, "Learning transferable architectures for scalable image recognition," in *Proceedings of the IEEE conference on Computer Vision and Pattern Recognition*, 2018, pp. 8697–8710.